



Electro-elastic Lamb waves in dielectric plates

Hannah Conroy Broderick^{a,*}, Luis Dorfmann^b, Michel Destrade^a

^a School of Mathematics, Statistics and Applied Mathematics, NUI Galway, University Road, Galway, Ireland

^b Department of Civil and Environmental Engineering, Tufts University, Medford, MA 02155, USA



ARTICLE INFO

Article history:

Received 25 March 2020

Received in revised form 28 April 2020

Accepted 16 May 2020

Available online 20 May 2020

Keywords:

Electro-elastic waves

Lamb waves

Electro-elasticity

Dielectric plates

Incremental formulations

ABSTRACT

We study the propagation of Lamb waves in soft dielectric plates subject to mechanical and electrical loadings and find the explicit expressions for the dispersion equations in the cases of neo-Hookean and Gent dielectrics. We elucidate the effects of the electric field, of the thickness-to-wavelength ratio, of pre-stress and of strain-stiffening on the wave characteristics.

© 2020 The Authors. Published by Elsevier Ltd. This is an open access article under the CC BY license (<http://creativecommons.org/licenses/by/4.0/>).

1. Introduction

Wave propagation in soft dielectric materials has been shown to depend on both the underlying deformation and the applied electric field for a variety of deformations and geometries.

Dorfmann and Ogden [1] derived the incremental formulation and showed the dependence of the surface wave velocity on the electric field in an electro-elastic half-space (voltage-controlled case). The case of a dielectric plate under plane strain was investigated by Shmuel et al. [2], who showed the effects of pre-stretch and applied electric displacement on the wave velocity (charge-controlled case). Ziser and Shmuel [3] investigated experimentally pre-stretched voltage-controlled films and found that the velocity of the fundamental flexural mode decreases with increasing voltage under plane strain. In a recent study, Wang et al. [4] considered the vibration of multi-layered compressible plates and highlighted interesting phenomena such as frequency jumping in plates undergoing snap-through.

There has been significant work on cylinders and tubes [5–9], showing that the velocity of the wave depends on the electric field and the direction in which it is applied, as well as the direction of propagation relative to the underlying electro-mechanical deformation. In particular, Wu et al. [9] highlighted the possibility of using wave propagation to detect defects or cracks in the material based on their analysis of circumferential waves.

The dependence of the wave velocity on the applied electric field suggests the possibility of controlling the velocity of

the propagating wave by applying an appropriate electric field [2,4]. It also paves the way for applying acoustic non-destructive evaluation techniques to dielectric plates.

Here, we first recall the equations governing the large deformation of a soft dielectric plate and then the subsequent propagation of small-amplitude Lamb waves, using incremental theory (Section 2). We write the equations of motion in the Stroh form, and then solve them for the neo-Hookean dielectric model (Section 3). We separate symmetric from antisymmetric modes of propagation to obtain explicit expressions for the corresponding dispersion equations, and for their limits in the long wavelength-thin plate and short wavelength-thick plate regimes. In Section 4, we solve the dispersion equations numerically to highlight the effects of loading and geometry on the wave propagation. We also use the Gent dielectric model to look at the effects of strain-stiffening and snap-through on the plate's acoustics.

2. Equations of motion

We use the incremental theory of electro-elasticity [1] to analyse wave propagation in a finitely deformed electro-active plate, within the context of the electro-acoustic approximation [10]. For completeness of presentation we first summarise the main parts of the theory.

The incremental (small-amplitude) mechanical displacement is denoted \mathbf{u} and the increments of the total nominal stress and of the Lagrangian forms of the electric displacement and the electric field are denoted by $\dot{\mathbf{T}}$, $\dot{\mathbf{D}}_L$, $\dot{\mathbf{E}}_L$, respectively. For an incompressible electro-elastic material the corresponding push-forward measures are obtained as

$$\dot{\mathbf{T}}_0 = \mathbf{F}\dot{\mathbf{T}}, \quad \dot{\mathbf{D}}_{L0} = \mathbf{F}\dot{\mathbf{D}}_L, \quad \dot{\mathbf{E}}_{L0} = \mathbf{F}^{-T}\dot{\mathbf{E}}_L, \quad (1)$$

* Corresponding author.

E-mail address: hannah.conroybroderick@nuigalway.ie (H. Conroy Broderick).

where \mathbf{F} is the deformation gradient. The incremental quantities satisfy the Lagrangian form of the governing equations

$$\text{Div} \dot{\mathbf{T}} = \rho \mathbf{u}_{,tt}, \quad \text{Div} \dot{\mathbf{D}}_L = 0, \quad \text{Curl} \dot{\mathbf{E}}_L = \mathbf{0}, \quad (2)$$

and, equivalently, their updated (Eulerian) forms

$$\text{div} \dot{\mathbf{T}}_0 = \rho \mathbf{u}_{,tt}, \quad \text{div} \dot{\mathbf{D}}_{L0} = 0, \quad \text{curl} \dot{\mathbf{E}}_{L0} = \mathbf{0}, \quad (3)$$

where ρ is the (constant) mass density per unit volume and $_{,t}$ denotes the time derivative.

With no external field and no applied mechanical traction the incremental boundary conditions have the simple forms

$$\dot{\mathbf{T}}^T \mathbf{N} = \mathbf{0}, \quad \dot{\mathbf{E}}_L \times \mathbf{N} = \mathbf{0}, \quad \dot{\mathbf{D}}_L \cdot \mathbf{N} = \dot{\sigma}_F, \quad (4)$$

where $\dot{\sigma}_F$ identifies an increment in the referential charge density on the electrodes attached to the major surfaces of the plate.

Superposed on the current configuration we consider an incremental motion, tracked by the incremental deformation gradient $\dot{\mathbf{F}}$, combined with an increment in the electric field $\dot{\mathbf{E}}_L$. This results in increments of the total nominal stress and of the Lagrangian electric displacement field as specified by the incremental forms of the constitutive equations [11].

In particular, for an incompressible material we have $\det \mathbf{F} = 1$ at all times. Then, $\dot{\mathbf{T}}$ and $\dot{\mathbf{D}}_L$ have the forms

$$\dot{\mathbf{T}} = \mathcal{A} \dot{\mathbf{F}} + \mathbb{A} \dot{\mathbf{E}}_L - \dot{p} \mathbf{F}^{-1} + p \mathbf{F}^{-1} \dot{\mathbf{F}} \mathbf{F}^{-1}, \quad (5)$$

and

$$\dot{\mathbf{D}}_L = -\mathbb{A}^T \dot{\mathbf{F}} - \mathbb{A} \dot{\mathbf{E}}_L, \quad (6)$$

where \mathcal{A} , \mathbb{A} , \mathbf{A} are, respectively, fourth-, third- and second-order electro-elastic moduli tensors, and p is a Lagrange multiplier due to incompressibility (and \dot{p} is its increment). The use of (1) gives the updated forms of the incremental constitutive equations

$$\dot{\mathbf{T}}_0 = \mathcal{A}_0 \mathbf{L} + \mathbb{A}_0 \dot{\mathbf{E}}_{L0} + p \mathbf{L} - \dot{p} \mathbf{I}, \quad (7)$$

and

$$\dot{\mathbf{D}}_{L0} = -\mathbb{A}_0^T \mathbf{L} - \mathbf{A}_0 \dot{\mathbf{E}}_{L0}, \quad (8)$$

where \mathbf{I} is the identity tensor and \mathbf{L} the gradient of the Eulerian version of the incremental displacement vector \mathbf{u} , see [12] for details. The latter satisfies the incremental incompressibility condition

$$\text{tr} \mathbf{L} = \text{div} \mathbf{u} = 0. \quad (9)$$

From (4) we find the updated incremental boundary conditions

$$\dot{\mathbf{T}}_0^T \mathbf{n} = \mathbf{0}, \quad \dot{\mathbf{E}}_{L0} \times \mathbf{n} = \mathbf{0}, \quad \dot{\mathbf{D}}_{L0} \cdot \mathbf{n} = \dot{\sigma}_{F0}, \quad (10)$$

where $\dot{\sigma}_{F0}$ is the Eulerian form of the charge density increment.

In what follows we focus attention on isotropic and incompressible electro-elastic materials with properties dependent on just two invariants, denoted I_1 and I_5 , and defined as

$$I_1 = \text{tr} \mathbf{C}, \quad I_5 = \mathbf{E}_L \cdot \mathbf{C}^{-1} \mathbf{E}_L, \quad (11)$$

where $\mathbf{C} = \mathbf{F}^T \mathbf{F}$ is the right Cauchy–Green deformation tensor.

We denote the lateral dimensions and the total thickness of an electroelastic plate in the undeformed configuration by $2L$ and $2H$, respectively. The deformed configuration is defined using the Cartesian coordinates (x_1, x_2, x_3) with x_2 oriented normal to the major surfaces. We focus on equi-biaxial deformations with principal stretches

$$\lambda_1 = \lambda_3 = \lambda, \quad \lambda_2 = \lambda^{-2}. \quad (12)$$

The deformed plate is then in the region

$$-\ell \leq x_1 \leq \ell, \quad -h \leq x_2 \leq h, \quad -\ell \leq x_3 \leq \ell, \quad (13)$$

where $2h = 2\lambda^{-2}H$ and $2\ell = 2\lambda L$ are the plate's dimensions in the deformed configuration.

In addition, a potential difference (voltage) is applied between the compliant electrodes attached at the top and bottom surfaces. The in-plane dimensions are much larger than the thickness and the edge effects can therefore be neglected. It follows that the accompanying electric and electric displacement fields have a single component each, denoted E_2 and D_2 , respectively, along the normal to the major surfaces of the plate. Eq. (1), specialised to the underlying configuration gives the Lagrangian counterparts as

$$E_{L2} = \lambda^{-2} E_2, \quad D_{L2} = \lambda^2 D_2. \quad (14)$$

while the invariants (11) have the simple forms

$$I_1 = 2\lambda^2 + \lambda^{-4}, \quad I_5 = \lambda^4 E_{L2}^2. \quad (15)$$

Superimposed on the underlying configuration we consider two-dimensional electro-elastic increments with components $u_1, u_2, \dot{E}_{L01}, \dot{E}_{L02}$, which depend on x_1, x_2 and t only.

Eq. (3)₃ suggests the introduction of a scalar function $\varphi = \varphi(x_1, x_2)$ such that

$$\dot{E}_{L01} = -\varphi_{,1}, \quad \dot{E}_{L02} = -\varphi_{,2}, \quad (16)$$

where the subscripts 1 and 2 following a comma denote partial derivatives with respect to x_1 and x_2 , respectively. Using (7) we find the non-zero incremental stress components $\dot{T}_{011}, \dot{T}_{012}, \dot{T}_{021}$, and \dot{T}_{022} and the non-zero incremental electric displacement components \dot{D}_{L01} and \dot{D}_{L02} from (8) [1,12,13]. Eq. (3)₁ and (3)₂ then specialise to

$$\begin{aligned} \dot{T}_{011,1} + \dot{T}_{021,2} &= \rho u_{1,tt}, \\ \dot{T}_{012,1} + \dot{T}_{022,2} &= \rho u_{2,tt}, \end{aligned} \quad (17)$$

$$\dot{D}_{L01,1} + \dot{D}_{L02,2} = 0, \quad (18)$$

together with the incompressibility condition (9)

$$u_{1,1} + u_{2,2} = 0. \quad (19)$$

It remains to specify the incremental boundary conditions (10)_{1,2} on the major surfaces $x_2 = \pm h$, as

$$\dot{T}_{021} = \dot{T}_{022} = 0, \quad \dot{E}_{L01} = 0, \quad (20)$$

while the boundary condition (10)₃ is not used, as we are considering a voltage-controlled plate.

Specifically, we seek solutions with sinusoidal dependence in the x_1 direction for the variables $u_1, u_2, \dot{D}_{L02}, \dot{T}_{021}, \dot{T}_{022}, \varphi$ in the form

$$\begin{aligned} \{u_1, u_2, \dot{D}_{L02}, \dot{T}_{021}, \dot{T}_{022}, \varphi\} \\ = \Re \{ [U_1, U_2, ik\Delta, ik\Sigma_{21}, ik\Sigma_{22}, \Phi] e^{ik(x_1 - vt)} \}, \end{aligned} \quad (21)$$

where the constant k is the wave number, v the wave speed and the amplitude functions $U_1, U_2, ik\Delta, ik\Sigma_{21}, ik\Sigma_{22}, \Phi$ are functions of kx_2 only.

In what follows, it is convenient to consider the variables U_1, U_2, Δ as the components of a generalised displacement vector \mathbf{U} , and the variables $\Sigma_{21}, \Sigma_{22}, \Phi$ as the components of a generalised traction vector \mathbf{S} . We find that the governing equations can then be arranged in the Stroh form

$$\boldsymbol{\eta}' = \mathbf{iN}\boldsymbol{\eta}, \quad (22)$$

where $\boldsymbol{\eta} = (\mathbf{U}, \mathbf{S})^T$ is the Stroh vector and the prime denotes differentiation with respect to kx_2 . The 6×6 matrix \mathbf{N} has the form

$$\mathbf{N} = \begin{bmatrix} \mathbf{N}_1 & \mathbf{N}_2 \\ \mathbf{N}_3 & \mathbf{N}_1^T \end{bmatrix}, \quad (23)$$

where the \mathbf{N}_i are 3×3 sub-matrices and $\mathbf{N}_2, \mathbf{N}_3$ are symmetric [13–15].

Next, we introduce shorthand notations for the coefficients in (7) and (8). For an energy function Ω that depends linearly on the invariants I_1 and I_5 , we use

$$\begin{aligned} a &= \mathcal{A}_{01212} = 2(\lambda^2 \Omega_1 + \lambda^2 E_{L2}^2 \Omega_5), \\ c &= \mathcal{A}_{02121} = 2\lambda^{-4} \Omega_1, \\ 2b &= \mathcal{A}_{01111} + \mathcal{A}_{02222} - 2\mathcal{A}_{01122} - 2\mathcal{A}_{01221} \\ &= 4(\lambda^2 - \lambda^{-4})^2 \Omega_{11} + a + c, \\ d &= \mathbb{A}_{0211} = -2\lambda^2 E_{L2} \Omega_5, \\ e &= \mathbb{A}_{0222} - \mathbb{A}_{0112} = 2d, \\ f &= \mathbf{A}_{011} = \mathbf{A}_{022} = 2\Omega_5, \end{aligned} \quad (24)$$

where $\Omega_j = \partial\Omega/\partial I_j$ for $j = 1, 5$. We also recall the connections [11]

$$\mathcal{A}_{0jilk} - \mathcal{A}_{0ijlk} = (\tau_{jl} + p\delta_{jl})\delta_{ik} - (\tau_{il} + p\delta_{il})\delta_{jk},$$

which for $\tau_{22} = 0$ results in $p = c$.

We introduce dimensionless versions of (24) as follows

$$\begin{aligned} \bar{a} &= a/\mu, & \bar{b} &= b/\mu, & \bar{c} &= c/\mu, \\ \bar{d} &= d/\sqrt{\mu\varepsilon}, & \bar{e} &= e/\sqrt{\mu\varepsilon}, & \bar{f} &= f/\varepsilon, \end{aligned} \quad (25)$$

where μ is the initial shear modulus associated with purely elastic deformations and ε is the (constant) electric permittivity. Together with the dimensionless field measures

$$\bar{E}_0 = E_{L2}\sqrt{\varepsilon/\mu}, \quad \bar{D}_0 = D_{L2}/\sqrt{\mu\varepsilon}, \quad (26)$$

and the non-dimensional components of the Stroh vector η ,

$$\begin{aligned} \bar{U}_i &= U_i, & \bar{\Delta} &= \Delta/\sqrt{\mu\varepsilon}, \\ \bar{\Sigma}_{2i} &= \Sigma_{2i}/\mu, & \bar{\Phi} &= \Phi\sqrt{\varepsilon/\mu}, \end{aligned} \quad (27)$$

we arrive at a non-dimensional version of the Stroh formulation (22) [13].

To derive the Stroh equations, we follow the procedure in [13]. As the only change in the governing equations from [13] is to the equilibrium equation for the stress, i.e. (3)₁ or equivalently (17), the only entries that change are those related to $\bar{\Sigma}_{21}$ and $\bar{\Sigma}_{22}$. As a result, \mathbf{N}_1 and \mathbf{N}_2 are identical to the forms derived in [13], and \mathbf{N}_3 becomes

$$\mathbf{N}_3 = \begin{bmatrix} \bar{e}^2 - 2(\bar{b} + \bar{c}) + \bar{v}^2 & 0 & -\bar{e} \\ \bar{f} & & \bar{f} \\ 0 & \bar{c} - \bar{a} + \bar{v}^2 & 0 \\ -\bar{e} & & 1 \\ -\bar{f} & & \bar{f} \end{bmatrix}, \quad (28)$$

where $\bar{v}^2 = \rho v^2/\mu$ is a non-dimensional version of v^2 .

3. Resolution for the neo-Hookean dielectric plate

We consider solutions in the form $\eta = \eta_0 e^{-p_k x_2}$, which reduce (22) to the eigen-problem $\mathbf{N}\eta_0 = ip\eta_0$. Hence, the eigenvalues and eigenvectors $p_j, \eta^{(j)}, j = 1, \dots, 6$ are determined by solving the characteristic equation

$$\det(\mathbf{N} - ip\mathbf{I}) = 0, \quad (29)$$

where \mathbf{I} is the 6×6 identity matrix. Note that the form of the solution used here is equivalent to the one in [13] using $p = iq$. It follows that the general solution for η has the form

$$\eta = \sum_{j=1}^6 c_j \eta^{(j)} e^{-p_j k x_2}, \quad (30)$$

where $c_j, j = 1, \dots, 6$ are constants to be determined by the boundary conditions (20).

To illustrate the solution, we now specialise the constitutive model $\Omega(I_1, I_5)$ to the neo-Hookean electroelastic form [16]

$$\Omega_{\text{NH}} = \frac{\mu}{2}(I_1 - 3) - \frac{\varepsilon}{2}I_5. \quad (31)$$

Then we find, using a Computer Algebra System, that solving the characteristic equation (29) results in

$$\begin{aligned} p_1 &= -p_4 = 1, & p_2 &= -p_5 = 1, \\ p_3 &= -p_6 = \lambda^2 \sqrt{\lambda^2 - \bar{v}^2}, \end{aligned} \quad (32)$$

with corresponding eigenvectors

$$\begin{aligned} \eta^{(1)} &= \begin{bmatrix} \lambda^4 \\ i\lambda^4 \\ 2\lambda^6 \bar{E}_0 \\ 2i \\ \lambda^4(\bar{v}^2 - \lambda^2 + \lambda^4 \bar{E}_0) - 1 \\ 0 \end{bmatrix}, \\ \eta^{(2)} &= \begin{bmatrix} i\lambda^6 \bar{E}_0^2 \\ -\lambda^6 \bar{E}_0^2 \\ i(\lambda^6 - \lambda^4 \bar{v}^2 + \lambda^8 \bar{E}_0^2 + 1) \\ \lambda^2 \bar{E}_0(\lambda^6 - \lambda^4 \bar{v}^2 - \lambda^8 \bar{E}_0^2 - 1) \\ 0 \\ \lambda^4(\bar{v}^2 - \lambda^2 + \lambda^4 \bar{E}_0^2) - 1 \end{bmatrix}, \\ \eta^{(3)} &= \begin{bmatrix} i\lambda^6 \sqrt{\lambda^2 - \bar{v}^2} \\ -\lambda^4 \\ i\lambda^8 \bar{E}_0 \sqrt{\lambda^2 - \bar{v}^2} \\ \lambda^4(\bar{v}^2 - \lambda^2 - \lambda^4 \bar{E}_0^2) - 1 \\ -2i\lambda^2 \sqrt{\lambda^2 - \bar{v}^2} \\ \lambda^6 \bar{E}_0 \end{bmatrix}, \end{aligned} \quad (33)$$

and $\eta^{(4)}, \eta^{(5)}, \eta^{(6)}$ are the respective complex conjugates of these three vectors.

The boundary conditions (20) on the surfaces $x_2 = \pm h$, in terms of the generalised traction vector \mathbf{S} require

$$\mathbf{S}(\pm kh) = \mathbf{0}. \quad (34)$$

These boundary conditions constitute six homogeneous equations that are conveniently represented as a 6×6 matrix equation. For a non-trivial solution the determinant of the matrix must vanish. The resulting equation can be factorised to give two independent equations, which identify the configurations in which antisymmetric and symmetric propagating waves may occur [13,15]. Specifically, for subsonic waves ($v < \lambda\sqrt{\mu/\rho}$, so that $\bar{v}^2 < \lambda^2$), we find the following explicit dispersion equations,

$$\begin{aligned} & \frac{(\lambda^6 - \lambda^4 \bar{v}^2 + 1)^2 - \lambda^8 (\lambda^6 - \lambda^4 \bar{v}^2 - 1) \bar{E}_0^2}{4\lambda^2 \sqrt{\lambda^2 - \bar{v}^2}} \\ &= \left[\frac{\tanh(kH \sqrt{\lambda^2 - \bar{v}^2})}{\tanh(kH \lambda^{-2})} \right]^{\pm 1}, \end{aligned} \quad (35)$$

where the exponents ± 1 correspond to antisymmetric and symmetric modes, respectively.

To evaluate the response in the short wavelength-thick plate and long wavelength-thin plate limits, we note that $kH = 2\pi H/\mathcal{L}$, where \mathcal{L} denotes the wavelength. Therefore, for short wavelengths-thick plates (Rayleigh surface waves), $kH \rightarrow \infty$

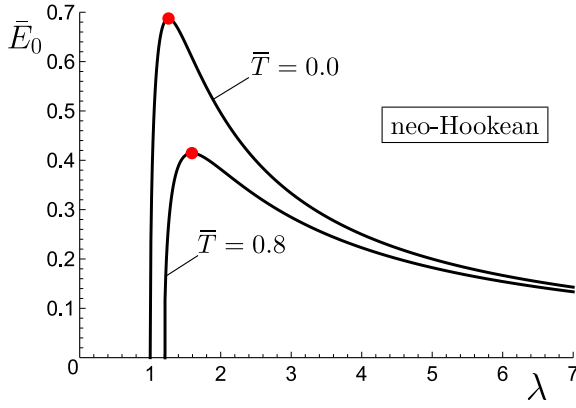


Fig. 1. The loading curve \bar{E}_0 against the in-plane stretch λ for a neo-Hookean electroelastic plate with no pre-stress ($\bar{T} = 0.0$, upper curve) and with pre-stress $\bar{T} = 0.8$ (lower curve). The field \bar{E}_0 increases initially with increasing values of λ , obtains its maximum \bar{E}_{\max} (marked by ‘●’) and decreases afterwards. As the pre-stress increases, \bar{E}_{\max} decreases, see [13] for a detailed discussion.

and Eq. (35) specialises to

$$\frac{(\lambda^6 - \lambda^4 \bar{v}^2 + 1)^2 - \lambda^8 (\lambda^6 - \lambda^4 \bar{v}^2 - 1) \bar{E}_0^2}{4\lambda^2 \sqrt{\lambda^2 - \bar{v}^2}} = 1. \quad (36)$$

In the long wavelength-thin plate limit, $kH \rightarrow 0$ and the anti-symmetric mode simplifies to

$$\lambda^8 \bar{E}_0^2 - \lambda^4 (\lambda^2 - \bar{v}^2) + 1 = 0, \quad (37)$$

while symmetric incremental modes occur when

$$\lambda^8 \bar{E}_0^2 - \lambda^4 (\lambda^2 - \bar{v}^2) - 3 = 0. \quad (38)$$

As expected, the above equations recover the purely elastic case [17] when $\bar{E}_0 = 0$ and the static electro-elastic case [13] when $\bar{v} = 0$.

When $\bar{v}^2 > \lambda^2$, using $\tanh(ix) = i \tan(x)$, we obtain

$$\frac{(\lambda^6 - \lambda^4 \bar{v}^2 + 1)^2 - \lambda^8 (\lambda^6 - \lambda^4 \bar{v}^2 - 1) \bar{E}_0^2}{4\lambda^2 \sqrt{\bar{v}^2 - \lambda^2}} = \mp \left[\frac{\tan(kH \sqrt{\bar{v}^2 - \lambda^2})}{\tanh(kH \lambda^{-2})} \right]^{\pm 1}, \quad (39)$$

where the upper and lower signs correspond to antisymmetric and symmetric modes, respectively. When $kH \ll 1$, Eq. (39) reduces to (37) for antisymmetric modes and to (38) for symmetric modes. When $kH \rightarrow \infty$, the limit is indeterminate, as the limit of $\tan(kH \sqrt{\bar{v}^2 - \lambda^2})$ is then undefined. This is expected because supersonic Rayleigh waves do not exist here; as seen in Fig. 4, \bar{v}^2 is always less than λ^2 for thick plates.

4. Numerical results and discussion

4.1. Neo-Hookean dielectric plate

On specialising to the constitutive model (31) and using the boundary condition $\tau_{22} = 0$, the in-plane nominal stress $T = \tau_{11}/\lambda = \tau_{33}/\lambda$ is obtained as

$$T = \mu (\lambda - \lambda^{-5}) - \varepsilon \lambda^3 E_{12}^2, \quad (40)$$

or, equivalently

$$\bar{E}_0 = \sqrt{\lambda^{-2} - \lambda^{-8} - \lambda^{-3} \bar{T}}, \quad (41)$$

where $\bar{T} = T/\mu$ is a dimensionless measure of the nominal stress. Relation (41) is illustrated by the loading curve \bar{E}_0 against the in-plane stretch λ , with pre-stresses $\bar{T} = 0$ and $\bar{T} = 0.8$ in

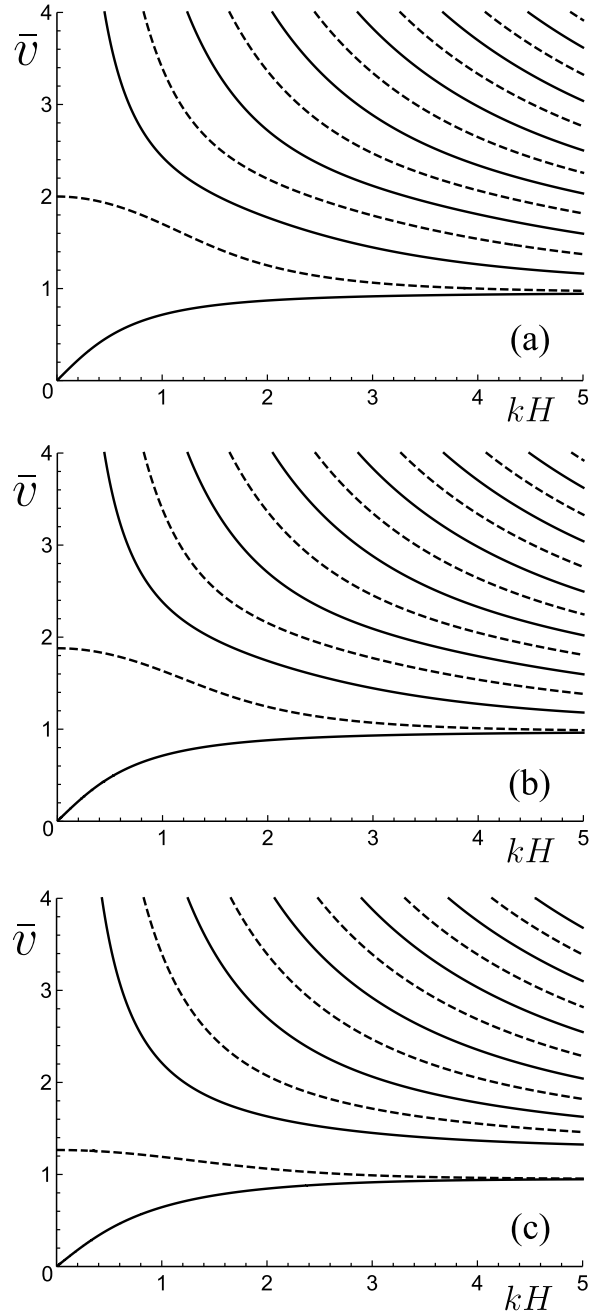


Fig. 2. The dimensionless Lamb wave speed $\bar{v} = v\sqrt{\rho/\mu}$ against kH of antisymmetric and symmetric modes shown by solid and dashed curves, respectively, for a neo-Hookean electroelastic plate with $\bar{T} = 0$. (a) Purely elastic un-stretched case $\bar{E}_0 = 0$, $\lambda = 1$, (b) Moderate electrical loading $\bar{E}_0 = 0.4$, $\lambda \simeq 1.03$, and (c) Maximal electrical loading $\bar{E}_0 = \bar{E}_{\max} = \sqrt{3}/2^{4/3}$, $\lambda = 2^{1/3}$.

Fig. 1. In the absence of pre-stress, the maximum value, $\bar{E}_{\max} = \sqrt{3}/2^{4/3} \simeq 0.69$, that the plate can support occurs at the critical stretch $\lambda = 2^{1/3} \simeq 1.26$, as shown by Zhao and Suo [16]. Loading curves for increasing amounts of prestress show a continuous reduction in the value of \bar{E}_{\max} , see for example [11,13,16].

We first consider a plate in the absence of pre-stress, i.e. we take $\bar{T} = 0.0$. To evaluate the effect of an electric field on the wave speeds of symmetric and antisymmetric modes, we must consider values of \bar{E}_0 and λ on the loading curve (41). Results show that for increasing values of \bar{E}_0 the overall trend of the curves is maintained as illustrated in Fig. 2. In particular, for $\bar{E}_0 = 0$ we recover the elastic results of an un-stretched plate [17].

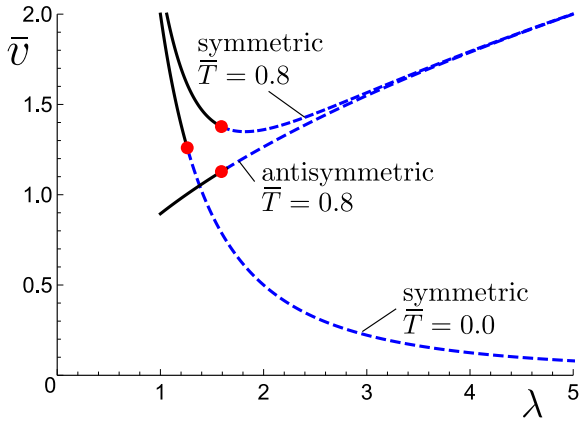


Fig. 3. The dimensionless wave speed $\bar{v} = v\sqrt{\rho/\mu}$ of the fundamental symmetric and antisymmetric modes against the stretch λ in the long wavelength-thin plate limit ($kH \rightarrow 0$) for a neo-Hookean dielectric plate with no pre-stress ($\bar{T} = 0.0$) and with pre-stress $\bar{T} = 0.8$. The wave speed when $\bar{E}_0 = \bar{E}_{\max}$, is marked by \bullet for each case. Beyond \bar{E}_{\max} the plate undergoes the pull-in instability, as indicated by the dashed portion of the curves.

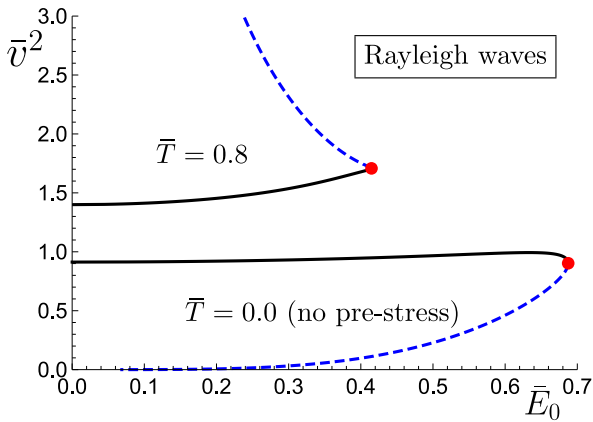


Fig. 4. The dimensionless squared Rayleigh wave speed $\bar{v}^2 = \rho v^2/\mu$ against \bar{E}_0 for a neo-Hookean electroelastic plate with $\bar{T} = 0.0$ and $\bar{T} = 0.8$, and $kH \rightarrow \infty$ (short wavelength-thick plate limit). The wave speed \bar{v}^2 when $\bar{E}_0 = \bar{E}_{\max}$ for each case is again marked by \bullet .

A notable feature of the effect of \bar{E}_0 on \bar{v} is the reduction of the speed of the fundamental symmetric mode in the long wavelength-thin plate limit, i.e. the mode with finite wave speed as $kH \rightarrow 0$. We can see this effect directly by substituting Eq. (41) at $\bar{T} = 0$ into (38), giving $\bar{v} = 2\lambda^{-2}$. The reduction in \bar{v} of the fundamental symmetric mode with increasing values of the stretch λ is shown in Fig. 3.

The corresponding Rayleigh wave speed is obtained from (36) using (41) to express the stretch λ in terms of the dimensionless field \bar{E}_0 . This is illustrated in Fig. 4 where \bar{E}_{\max} is again indicated by \bullet . For $\bar{E}_0 = 0$, we recover Lord Rayleigh's result [18] of the purely elastic surface wave, $\bar{v}^2 = 0.9126$. As \bar{E}_0 increases with increasing λ , the Rayleigh wave speed increases as well until it reaches its maximum at $\bar{E}_0 \simeq 0.6329$, $\lambda \simeq 1.1251$, before \bar{E}_{\max} is reached. The speed then begins to decrease and past \bar{E}_{\max} , when the electric field decreases at increased stretch, it decreases rapidly to zero.

These trends are in contrast to those of Shmuel et al. [2], who found that both the Rayleigh wave speed and the thin-plate limit of the fundamental symmetric mode increase monotonically with increased electric displacement. However, they considered a charge-controlled dielectric plate under the influence of a plane

strain deformation, and so we cannot perform a direct comparison. Instead we can compare their results with the case of a voltage-controlled plate under plane strain. In that case we also find that the fundamental symmetric mode in the long-wavelength limit decreases monotonically. We can again see this by substituting the loading curve into the thin-plate limit giving $\bar{v} = 2\lambda^{-1}$. The Rayleigh wave speed follows a similar trend to the equi-biaxial case, increasing towards a maximum as the electric field increases. The speed then decreases asymptotically, corresponding to the asymptote of the loading curve.

4.2. Pre-stressed dielectric plate

We now investigate the effect of pre-stress on wave propagation in a neo-Hookean dielectric plate. We use a pre-stress of $T = 0.8$ as a representative example. In that case the corresponding pre-stretch is $\lambda \simeq 1.2$ in the absence of an electric field, and the loading curve reaches its maximum at $\bar{E}_0 = \bar{E}_{\max} \simeq 0.4148$, $\lambda \simeq 1.5916$, as seen in Fig. 1.

We again consider values of \bar{E}_0 and λ along the loading curve (41), and plot the dispersion curves (35) when $\bar{T} = 0.8$ in Fig. 5. When $\bar{E}_0 = 0$, the dispersion curves recover the corresponding curves in the elastic case (see, for example, [17] for similar plots at different values of pre-stress). As before, as \bar{E}_0 increases towards \bar{E}_{\max} , the overall trend of the $\bar{E}_0 = 0$ curve is maintained. The symmetric long-wave limit decreases and the thick-plate limit increases as \bar{E}_0 is increased towards \bar{E}_{\max} , following similar trends to the case without pre-stress (Figs. 3, 4).

The major difference between the pre-stressed and non-pre-stressed cases is the behaviour in the long wavelength-thin plate regime: once a pre-stress is introduced, the speed of the anti-symmetric modes in this limit become non-zero. As the stretch is increased, the speed of the fundamental antisymmetric mode in that limit also increases (Fig. 3), which can be seen explicitly by substituting the loading curve (41) into Eq. (37), giving $\bar{v} = \sqrt{\lambda\bar{T}}$, a monotonically increasing function of λ for any positive \bar{T} . We note that in the plane strain case, the antisymmetric long wavelength limit becomes $\bar{v} = \sqrt{\lambda^{-1}\bar{T}}$, a monotonically decreasing function for any positive \bar{T} , corresponding to the slowing found experimentally by Ziser and Shmuel [3].

By substituting (41) into (38) we see that the limit for the symmetric modes becomes

$$\bar{v} = \sqrt{4\lambda^{-4} + \lambda\bar{T}}, \quad (42)$$

in the pre-stressed case. As λ increases beyond $\lambda \simeq 1.5916$, the $\lambda\bar{T}$ term dominates and the speed in the long wavelength-thin plate limit begins to increase, unlike in the case without pre-stress where it decreases monotonically. As a result, for large λ the symmetric and antisymmetric thin-plate/long wavelength limits converge to the same value ($\bar{v} = \sqrt{\lambda\bar{T}}$), as seen in Fig. 3.

The short wavelength-thick plate limit ($kH \gg 1$) also deviates from the trend in the case with no pre-stress (Fig. 4). Initially, the wave speed \bar{v}^2 increases as the electric field increases, until it reaches the maximum $\bar{E}_0 \simeq 0.4148$, as before. At this point, the curve changes suddenly and the speed begins to increase, as the electric field decreases with increased stretch. At lower values of pre-stress (not shown here), the wave speed initially follows a similar trend as in Fig. 4, and begins to decrease, after which it begins to increase, as in the $\bar{T} = 0.8$ case.

4.3. Gent dielectric plate

In this section we investigate wave propagation characteristics in a plate made of an electro-elastic, strain-stiffening Gent dielectric, with energy function

$$\Omega_G = -\frac{\mu J_m}{2} \log \left[1 - \frac{(I_1 - 3)}{J_m} \right] - \frac{\varepsilon}{2} I_5, \quad (43)$$

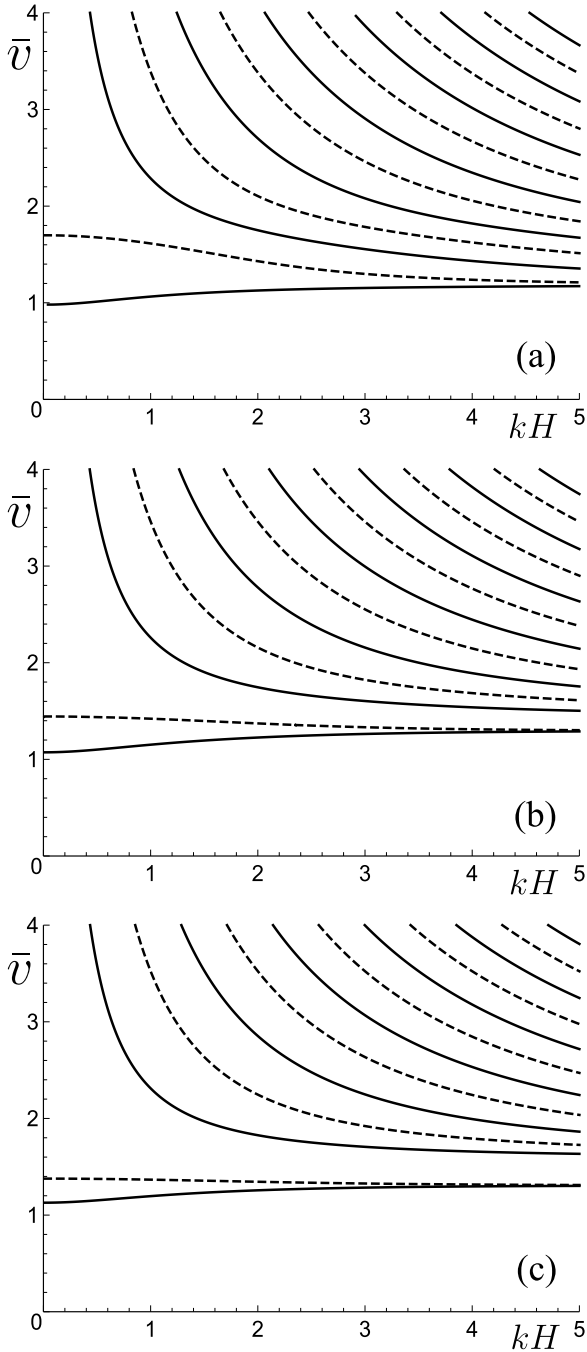


Fig. 5. The dimensionless wave speed $\bar{v} = v\sqrt{\rho/\mu}$ against kH of antisymmetric (solid) and symmetric (dashed) modes for a pre-stressed neo-Hookean electroelastic plate, with $\bar{T} = 0.8$. (a) The elastic case with $\bar{E}_0 = 0$, $\lambda \simeq 1.2$, (b) Moderate electric field $\bar{E}_0 = 0.4$, $\lambda \simeq 1.4387$, and (c) The maximal electric field $\bar{E}_0 \simeq 0.4148$, $\lambda \simeq 1.5916$.

where the invariants I_1, I_5 are given in (15) and J_m is a material constant, capturing strain-stiffening effects at large stretches. Following the work of Dorfmann and Ogden [11,19] we use the specific value $J_m = 97.2$, which is typical for soft rubber.

The in-plane nominal stress is now connected to the stretch λ and the Lagrangian electric field by

$$T = \mu \frac{\lambda - \lambda^{-5}}{1 - (2\lambda^2 + \lambda^{-4} - 3)/J_m} - \varepsilon \lambda^3 E_{L2}^2, \quad (44)$$

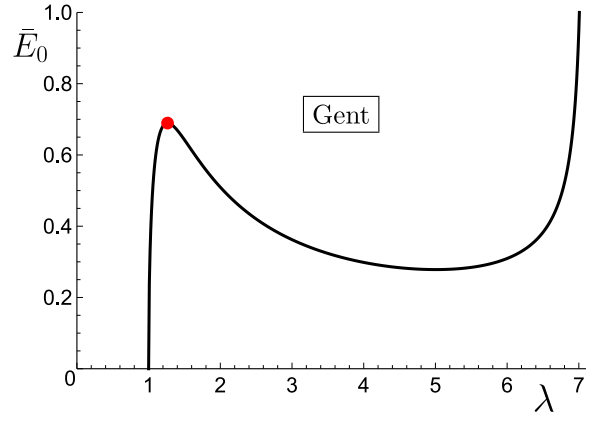


Fig. 6. The loading curve \bar{E}_0 against the in-plane stretch λ for a Gent electro-elastic plate with $J_m = 97.2$ and $\bar{T} = 0$.

leading to the following non-dimensional form of the loading curve

$$\bar{E}_0 = \sqrt{\frac{\lambda^{-2} - \lambda^{-8}}{1 - (2\lambda^2 + \lambda^{-4} - 3)/J_m}} - \lambda^{-3}\bar{T}. \quad (45)$$

Fig. 6 illustrates relation (45) for the special case when $\bar{T} = 0$, highlighting the snap-through instability. The field \bar{E}_0 increases with increasing λ and reaches a local maximum, $\bar{E}_{\max} \simeq 0.689$ when $\lambda \simeq 1.264$. The stretch then increases with constant electric field until it reaches $\lambda \simeq 6.926$, after which the stretch and electric field increase together, i.e. the snap-through instability, see [11,13] for detailed discussions.

The explicit expression of the Stroh matrix \mathbf{N} for the Gent dielectric is obtained by following the steps identified in Section 3 with the derivatives in (24) evaluated using the energy function (43). Then, the solution of (29) gives the eigenvalues

$$p_1 = 1, \quad (46)$$

$$p_{2,3} = \frac{1}{2} \sqrt{(1 + \kappa)^2 + 2(\lambda^4 - \lambda^{-2})^2 \frac{\bar{\Omega}_{11}}{\bar{\Omega}_1}} \pm \frac{1}{2} \sqrt{(1 - \kappa)^2 + 2(\lambda^4 - \lambda^{-2})^2 \frac{\bar{\Omega}_{11}}{\bar{\Omega}_1}},$$

with

$$p_4 = -p_1, \quad p_5 = -p_2, \quad p_6 = -p_3, \quad (47)$$

where

$$\kappa = \sqrt{\lambda^6 - \frac{\lambda^4 \bar{v}^2}{2\bar{\Omega}_1}}, \quad (48)$$

and

$$\bar{\Omega}_1 = \frac{1}{2} \frac{J_m}{3 + J_m - I_1}, \quad \bar{\Omega}_{11} = \frac{1}{2} \frac{J_m}{(3 + J_m - I_1)^2}, \quad (49)$$

are the (non-dimensional) derivatives of (43) with respect to I_1 . In addition, the solution of (29) gives the corresponding eigenvectors

$$\eta^{(1)} = \begin{bmatrix} 0 \\ 0 \\ -i \\ -\lambda^2 \bar{E}_0 \\ -i\lambda^2 \bar{E}_0 \\ 1 \end{bmatrix}, \quad (50)$$

$$\eta^{(2)} = \begin{bmatrix} i\lambda^4 p_2 \\ -\lambda^4 \\ i\lambda^6 \bar{E}_0 p_2 \\ -(2\bar{\Omega}_1(p_2^2 + 1) + \lambda^8 \bar{E}_0^2) \\ -i(2\bar{\Omega}_1(\lambda^6 + p_2^2) - \lambda^4 \bar{v}^2) / p_2 \\ \lambda^6 \bar{E}_0 \end{bmatrix},$$

$$\eta^{(3)} = \begin{bmatrix} i\lambda^4 p_3 \\ -\lambda^4 \\ i\lambda^6 \bar{E}_0 p_3 \\ -(2\bar{\Omega}_1(p_3^2 + 1) + \lambda^8 \bar{E}_0^2) \\ -i(2\bar{\Omega}_1(\lambda^6 + p_3^2) - \lambda^4 \bar{v}^2) / p_3 \\ \lambda^6 \bar{E}_0 \end{bmatrix},$$

with $\eta^{(4)}$, $\eta^{(5)}$, $\eta^{(6)}$ their complex conjugates.

For antisymmetric wave modes and $\bar{v}^2/(2\bar{\Omega}_1) < \lambda^2$ we find the following dispersion equation

$$\begin{aligned} & \kappa(p_2^2 - p_3^2)\lambda^8 \bar{E}_0^2 \tanh(\lambda^{-2}kH) + p_3(p_2^2 + 1) \\ & \times [2\bar{\Omega}_1(\lambda^6 + p_2^2) - \lambda^4 \bar{v}^2] \tanh(\lambda^{-2}p_2kH) \\ & - p_2(p_2^2 + 1)[2\bar{\Omega}_1(\lambda^6 + p_3^2) - \lambda^4 \bar{v}^2] \tanh(\lambda^{-2}p_3kH) = 0, \end{aligned} \quad (51)$$

where the in-plane stretch λ and the field \bar{E}_0 are connected by (45). The corresponding equation for symmetric modes is obtained from (51) by replacing the hyperbolic function \tanh with \coth . Note that for $\bar{v}^2/(2\bar{\Omega}_1) > \lambda^2$ the eigenvalue p_2 is imaginary and, therefore, to obtain real solutions the dispersion equation for antisymmetric and symmetric modes must be multiplied by the imaginary unit i .

Again the dispersion relation (51) recovers the electrostatic case when $\bar{v} = 0$ and the elastic case when $\bar{E}_0 = 0$.

When $kH \gg 1$ (Rayleigh waves), Eq. (51) and its symmetric counterpart tend to

$$\begin{aligned} & \lambda^8 \kappa(p_2 + p_3)\bar{E}_0^2 + \lambda^4 \bar{v}^2(p_2^2 + p_3^2 + 1 + \kappa) \\ & - 2[\lambda^6(p_2 + p_3)^2 + (1 - \kappa)(\lambda^6 - \kappa)]\bar{\Omega}_1 = 0. \end{aligned} \quad (52)$$

The Rayleigh wave speed \bar{v}^2 in (52) is evaluated using (45) and depicted in Fig. 7 against the field \bar{E}_0 . For the purely elastic case with no pre-stress ($\bar{E}_0 = 0$, $\lambda = 1$) we again recover the Rayleigh wave speed of a linear incompressible solid [18], $\bar{v}^2 = 0.9126$ (see [20,21] for Rayleigh waves in a deformed, purely elastic, Gent material). Initially, the wave speed follows a similar trend as in the neo-Hookean case (Fig. 4), but shortly after the snap-through point ($E_0 \simeq 0.689$) the speed begins to increase substantially with decreasing electric field, due to the exponential stiffening of the material with increasing stretch after the snap-through instability.

When the plate undergoes the snap-through instability, the Rayleigh wave speed is increased by more than a thousandfold, with a jump to the value $\bar{v}^2 \simeq 1,045$, and then increases further with the electric field. Wang et al. [4] found a similar phenomenon, with natural frequency jumping occurring during snap-through. However, they considered a pre-stretched plate and a compressible energy density function, which results in a smaller increase in stretch due to the snap-through instability than when incompressibility is enforced and when there is no pre-stretch. For the Gent dielectric considered here, the increase in stretch is very large (about 600%, see Fig. 6), which explains the very large jump in speed (or frequency).

In the long wavelength-thin plate limit $kH \rightarrow 0$, the dispersion equation for antisymmetric incremental modes simplifies to

$$\lambda^8 \bar{E}_0^2 - 2\bar{\Omega}_1(\lambda^6 - 1) + \lambda^4 \bar{v}^2 = 0, \quad (53)$$

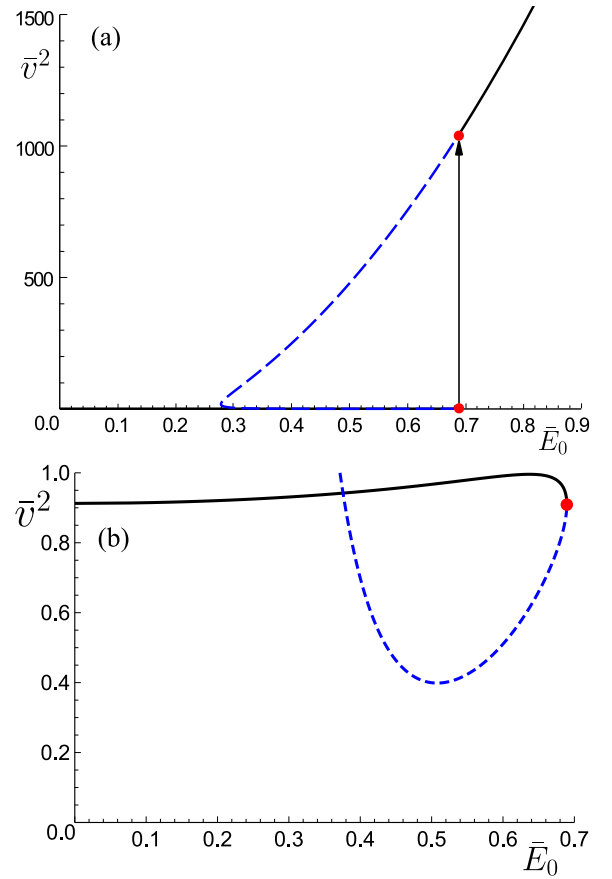


Fig. 7. The dimensionless Rayleigh wave speed \bar{v}^2 against \bar{E}_0 for a Gent electro-elastic plate with no pre-stress ($\bar{T} = 0.0$) in the short wavelength-thick plate limit. (a) The jump in velocity due to snap-through. (b) The Rayleigh wave speed before the snap-through instability. The values of \bar{v}^2 corresponding to $\bar{E}_0 = \bar{E}_{\max} = 0.689$ are denoted by \bullet .

while the wave speed for symmetric modes is governed by

$$\lambda^{12} \bar{E}_0^2 + \lambda^8 \bar{v}^2 - 4\bar{\Omega}_{11}(\lambda^6 - 1)^2 - 2\lambda^4 \bar{\Omega}_1(\lambda^6 + 3) = 0. \quad (54)$$

It is easy to check that Eq. (53) gives the trivial solution $\bar{v} = 0$ for \bar{E}_0 and λ taken on the loading curve (45), while Eq. (54) simplifies to

$$8\lambda^4 \bar{\Omega}_1 + 4\bar{\Omega}_{11}(\lambda^6 - 1)^2 - \lambda^8 \bar{v}^2 = 0. \quad (55)$$

The corresponding non-dimensionalised velocity \bar{v} of the symmetric fundamental mode in the limit $kH \rightarrow 0$ against the in-plane stretch λ is shown in Fig. 8. As λ increases towards the snap-through point ($\lambda \simeq 1.264$), the speed of the symmetric fundamental mode decreases, as in the neo-Hookean case (Fig. 3). When $\lambda \simeq 1.9$, the speed begins to increase as the stretch increases, and continues to increase monotonically beyond the past snap-through point ($\lambda \simeq 6.926$). This effect is due to the stiffening after the snap-through instability.

To illustrate the effect of the snap-through instability on the wave velocity, we plot the dispersion relation (51) at the snap-through point ($\bar{E}_0 = \bar{E}_{\max} \simeq 0.689$, $\lambda \simeq 1.264$) and the past snap-through point where $\lambda \simeq 6.926$ in Fig. 9. At the snap-through point ($\lambda \simeq 1.264$), the curves follow the same trend as those of the neo-Hookean energy density function, see Fig. 2c. After the snap-through has taken place ($\lambda \simeq 6.926$), the velocity increases dramatically. The speeds of the symmetric modes in the $kH \ll 1$ and $kH \gg 1$ regimes have both increased, but the overall trend of the fundamental modes remains the same. The dramatic

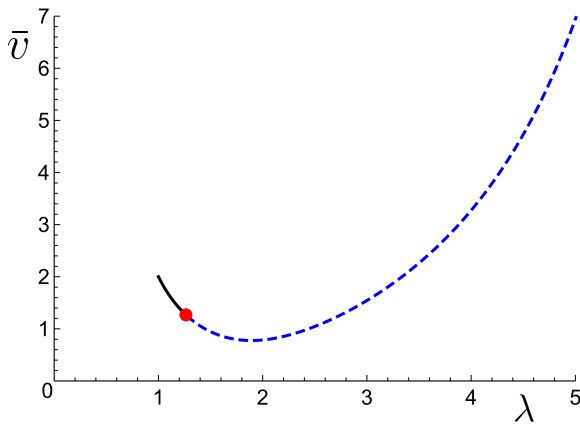


Fig. 8. The dimensionless velocity \bar{v} of the fundamental symmetric mode in the long wavelength-thin plate limit ($kH \rightarrow 0$) against the stretch λ for a Gent electro-elastic plate. The wave speed marked by \bullet occurs when $\lambda = 1.264$ and $\bar{E}_0 = \bar{E}_{\max} = 0.689$.

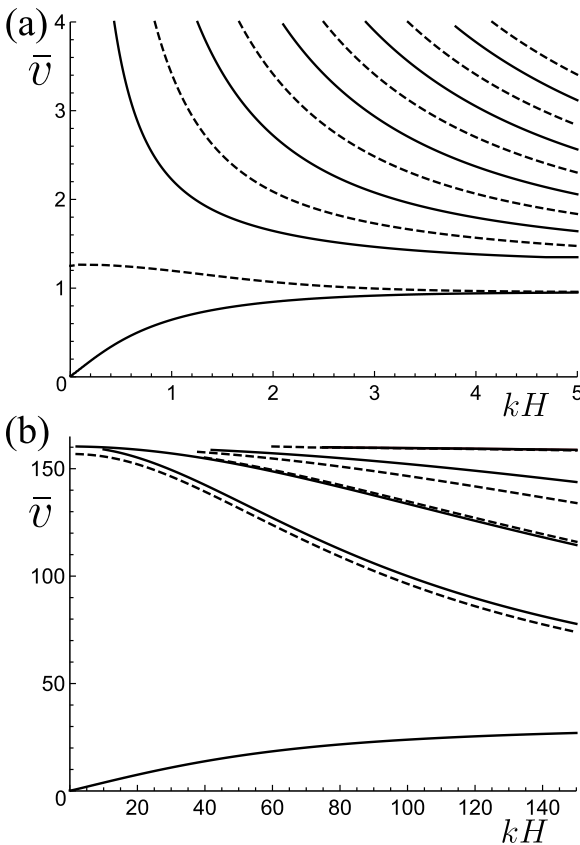


Fig. 9. The non-dimensionalised Lamb wave speed $\bar{v} = v\sqrt{\rho/\mu}$ against kH of antisymmetric and symmetric modes shown by solid and dashed curves, respectively, for a Gent electroelastic plate with no pre-stress ($\bar{T} = 0.0$). (a) The response at the snap-through point where $\bar{E}_{\max} = 0.689$ and $\lambda = 1.264$, and (b) The past snap-through point where $\bar{E}_{\max} = 0.689$ and $\lambda = 6.926$, see Fig. 6.

increase in the values of the speed is due to the very large stretch at the past snap-through point, where the plate is under large strain and is much stiffened.

The first antisymmetric and symmetric modes also converge to the short-wave limit much slower than in all other cases. This is again due to the large stretch, as the competition between kH and λ^{-2} is greater for large λ .

5. Concluding remarks

In this paper, we investigated Lamb wave characteristics in the presence of an electric field generated by a potential difference between two flexible electrodes mounted on the major surfaces of a dielectric plate. The incremental governing equations and the electrical and mechanical boundary conditions are given in Stroh form and solved numerically for neo-Hookean and Gent dielectric models. The dispersion equation is factorised to give two independent equations, which identify the configurations where antisymmetric and symmetric propagating waves may occur. Explicit expressions of the dispersion equations for the short wavelength-thick plate and long wavelength-thin plate limits are obtained. In particular, we investigated the effects of plate thickness, of the electric field, of an in-plane pre-stress and of stretch-stiffening on the wave characteristics.

Declaration of competing interest

The authors declare that they have no known competing financial interests or personal relationships that could have appeared to influence the work reported in this paper.

Acknowledgements

This work is supported by a Government of Ireland Postgraduate Scholarship from the Irish Research Council, Ireland (Project GOIPG/2016/712).

References

- [1] A. Dorfmann, R.W. Ogden, Electroelastic waves in a finitely deformed electroactive material, *IMA J. Appl. Math.* 75 (2010) 603–636.
- [2] G. Shmuel, M. Gei, G. deBotton, The Rayleigh–Lamb wave propagation in dielectric elastomer layers subjected to large deformations, *Int. J. Nonlinear Mech.* 47 (2012) 307–316.
- [3] Y. Ziser, G. Shmuel, Experimental slowing of flexural waves in dielectric elastomer films by voltage, *Mech. Res. Commun.* 85 (2017) 64–68.
- [4] Y. Wang, Z. Li, W.Q. Chen, C. Zhang, J. Zhu, Free vibration an active control of pre-stretched multilayered electroactive plates, *Int. J. Solids Struct.* 180–181 (2019) 108–124.
- [5] W.Q. Chen, H.H. Dai, Waves in pre-stretched incompressible soft electroactive cylinders: Exact solution, *Acta Mech. Solida Sin.* 25 (2012) 530–541.
- [6] L. Dorfmann, R.W. Ogden, Waves and vibrations in a finitely deformed electroelastic circular cylindrical tube, *Proc. R. Soc. Lond. Ser. A Math. Phys. Eng. Sci.* 476 (2020) 20190701.
- [7] G. Shmuel, G. deBotton, Axisymmetric wave propagation in finitely deformed dielectric elastomer tubes, *Proc. R. Soc. Lond. Ser. A Math. Phys. Eng. Sci.* 469 (2013) 20130071.
- [8] Y.P. Su, H.M. Wang, C.L. Zhang, W.Q. Chen, Propagation of non-axisymmetric waves in an infinite soft electroactive hollow cylinder under uniform biasing fields, *Int. J. Solids Struct.* 81 (2016) 262–273.
- [9] B. Wu, Y.P. Su, W.Q. Chen, C.L. Zhang, On guided circumferential waves in soft electroactive tubes under radially inhomogeneous biasing fields, *J. Mech. Phys. Solids* 99 (2017) 116–145.
- [10] R.W. Ogden, Incremental elastic motions superimposed on a finite deformation in the presence of an electromagnetic field, *Internat. J. Non-Linear Mech.* 44 (2009) 570–580.
- [11] L. Dorfmann, R.W. Ogden, Instabilities of soft dielectrics, *Phil. Trans. R. Soc. A* 377 (2019) 20180077.
- [12] L. Dorfmann, R.W. Ogden, *Nonlinear Theory of Electroelastic and Magnetoelastic Interactions*, Springer, New York, 2014.
- [13] Y. Su, H. Conroy Broderick, W. Chen, M. Destrade, Wrinkles in soft dielectric plates, *J. Mech. Phys. Solids* 119 (2018) 298–318.
- [14] A.L. Shuvalov, On the theory of wave propagation in anisotropic plates, *Proc. R. Soc. A* 456 (2000) 2197–2222.
- [15] L. Dorfmann, R.W. Ogden, Electroelastic plate instabilities based on the Stroh method in terms of the energy function $\Omega^*(\mathbf{F}, \mathbf{D}_\perp)$, *Mech. Res. Commun.* 96 (2019) 67–74.
- [16] X. Zhao, Z. Suo, Method to analyze electromechanical stability of dielectric elastomers, *Appl. Phys. Lett.* 91 (2007) 061921.

- [17] R.W. Ogden, D.G. Roxburgh, The effect of pre-stress on the vibration and stability of elastic plates, *Internat. J. Engrg. Sci.* 31 (1993) 1611–1639.
- [18] Lord Rayleigh, On waves propagated along the plane surface of an elastic solid, *Proc. Lond. Math. Soc.* 17 (1885) 4–11.
- [19] L. Dorfmann, R.W. Ogden, Nonlinear response of an electroelastic spherical shell, *Internat. J. Engrg. Sci.* 85 (2014) 163–174.
- [20] M. Destrade, N.H. Scott, Surface waves in a deformed isotropic hyperelastic material subject to an isotropic internal constraint, *Wave Motion* 40 (2004) 347–357.
- [21] M. Destrade, R.W. Ogden, Surface waves in a stretched and sheared incompressible elastic material, *Int. J. Non-Linear Mech.* 40 (2005) 241–253.